JBC Papers in Press. Published on May 2, 2019 as Manuscript RA118.006551
The latest version is at http://www.jbc.org/cgi/doi/10.1074/jbc.RA118.006551

E46K-like α-synuclein mutants increase lipid interactions and disrupt membrane selectivity

Matteo Rovere[1], Alex E. Powers[1], Haiyang Jiang[1,§], Julia C. Pitino[1,§], Luis Fonseca-Ornelas[1], Dushyant S. Patel[1], Alessandro Achille[2], Ralf Langen[3], Jobin Varkey[3], Tim Bartels[1,4,*].

From the [1]Ann Romney Center for Neurologic Diseases, Brigham and Women's Hospital and Harvard Medical School, Boston MA, 02115, USA; the [2]Department of Computer Science, University of California, Los Angeles, Los Angeles CA, 90095, USA; the [3]Zilkha Neurogenetic Institute, University of Southern California, Los Angeles CA, 90033, USA; [4]the Dementia Research Institute, University College London, London, WC1E 6BT, UK

Running Title: *E46K-like α-synuclein mutants disrupt membrane selectivity*

[§]These authors contributed equally to this work.

*To whom correspondence should be addressed: Dementia Research Institute, University College London, London, Gower Street, Cruciform Building Wing 2.4, WC1E 6BT, UK. Phone: +44-20-31086814; E-mail: t.bartels@ucl.ac.uk

Keywords: α-synuclein, Parkinson's Disease, Neurodegeneration, Intrinsically Disordered Proteins, 11/3 Helix, Protein-Lipid Interaction, Circular Dichroism, Isothermal Titration Calorimetry, Small Unilamellar Vesicles, Large Unilamellar Vesicles

ABSTRACT

Parkinson's disease (PD) is one of the most common neurodegenerative disorders and both genetic and histopathological evidence have implicated the ubiquitous presynaptic protein α-synuclein (αSyn) in its pathogenesis. Recent work has investigated how disrupting αSyn's interaction with membranes triggers trafficking defects, cellular stress, and apoptosis. Special interest has been devoted to a series of mutants exacerbating the effects of the E46K mutation (associated with autosomal dominant PD) through homologous E-to-K substitutions in αSyn's N-terminal region (*i.e.* E35K, E61K). Such E46K-like mutants have been shown to cause dopaminergic neuron loss and severe, yet L-DOPA–responsive, motor defects in mouse overexpression models, presenting enormous translational potential for PD and other "synucleinopathies". In this work, using a variety of biophysical techniques, we characterize the molecular pathology of E46K-like αSyn mutants by studying their structure and membrane-binding and remodeling abilities. We find that, although a slight increase in the mutants' avidity for synaptic vesicle–like membranes can be detected, most of their deleterious effects are connected to their complete disruption of αSyn's curvature selectivity. Indiscriminate binding can shift αSyn's subcellular localization away from its physiological interactants at the synaptic bouton toward trafficking vesicles and organelles, as observed in E46K-like cellular and murine models, as well as in human pathology. In conclusion, our findings suggest that a loss of curvature selectivity, rather than increased membrane affinity, could be the critical dyshomeostasis in synucleinopathies.

Parkinson's disease (PD) is a progressive neurodegenerative disorder, characterized in its early stages by resting tremor, bradykinesia and rigidity due to the loss of dopaminergic neurons in the substantia nigra (1). Its prevalence in industrialized countries is estimated at 1% in people over 60 years of age, making it the second most common neurodegenerative disorder after Alzheimer's disease (2). α-Synuclein (αSyn), a small presynaptic protein ubiquitously expressed in nervous tissue (3), has long been considered a key player in the pathogenesis of PD, as supported by both genetic and histopathologic evidence (4).

Its role in neuronal physiology, while still debated, has been tied to the maintenance of synaptic homeostasis (5, 6). These mechanisms are especially important in dopaminergic neurons, which exhibit high-frequency activity bursts (7).

One of the recurring themes of αSyn biology is its affinity for lipid interfaces and how such interplay shapes its function and dysfunction. While αSyn has been classically considered an intrinsically disordered protein (IDP) (8, 9), its N-terminal region contains seven imperfect 11-mer repeats (with the consensus XKTKEGVXXXX), homologous to those of apolipoproteins (10–12). In fact, upon interaction with liposomes and micelles, αSyn undergoes a coil-to-helix transition and binds robustly to curved negatively charged interfaces (13, 14). In particular, its specificity for lipid bilayers similar in charge and curvature to those of synaptic vesicles (15) is attained by virtue of the periodic arrangement of mildly hydrophobic and hydrophilic amino acid side chains (16). In addition, the numerous lysines in the N-terminal region mediate the formation of ionic bridges with the charged heads of negative membranes (17). αSyn's N-terminus has also been shown to be critical for its subcellular localization to the presynaptic terminals (18) and its partitioning between the cytosol and membranes, regulated by electrical activity (19).

Along with its role in cellular physiology, the lipid-binding ability of αSyn's N-terminal region has also been implicated in the pathogenesis of neurodegeneration (20). Overexpression of αSyn and its mutants associated with autosomal dominant PD (fPD) in yeast and mammalian cell models severely compromises vesicle trafficking and protein clearance through abnormal membrane association (21–23). In addition, vesicle and organelle clusters have been recognized as prominent features of Lewy pathology (24).

Recent work has shown that modifications in αSyn's repeats which enhance the amphipathic nature of its membrane-binding helix modulate toxicity upon overexpression (25, 26). Inserting either more hydrophobic residues on the largely apolar face of the helix or charged residues on the cytosol-exposed side appears to increase the ability of αSyn mutants to induce toxicity and cluster a variety of intracellular vesicles and organelles into αSyn-rich inclusions. Among these mutants, E-to-K mutations homologous to the fPD-associated E46K mutation (27) (e.g. E35K, E61K) are of particular interest because of their direct connection to disease and their robust toxicity in cellular models (28). Readouts of cellular toxicity (e.g. viability, apoptotic markers) and their ability to cluster vesicles correlate with the number of E-to-K substitutions, suggesting a common molecular mechanism between the E46K mutation and these "exacerbated" E46K-like mutants. In addition, such mutants have been shown to markedly decrease the ratio between aggregation-resistant αSyn tetramers (29) and aggregation-prone monomers, whose imbalance has been proposed as one of the molecular mechanisms underlying disease inception (28, 30). Lastly, heterozygous transgenic mice overexpressing E46K-like αSyn mutants present a robust and progressive PD-like phenotype, with severe tremor and gait deficits (partially rescued by L-DOPA administration), loss of dopaminergic neurons and formation of protease-resistant αSyn-rich inclusions in neuronal bodies (31).

In this work we characterize the lipid-binding and lipid-remodeling abilities of three of these E-to-K mutants (E46K, "K"; E35,46K, "2K"; and E35,46,61K, "3K", Fig. 1) using a variety of biophysical methods. Through comparisons between multiple E46K-like substitutions in αSyn's N-terminal region, we draw insights both on the molecular pathology of E46K (and E46K-like) αSyn mutants and on the structure of membrane-bound αSyn.

Results

E46K-like mutants increase N-to-C interactions and coil compactness

In order to characterize whether the E-to-K mutations induced any change in the structure of the lipid-unbound protein, Circular Dichroism (CD) spectra of the recombinant mutants in buffer were measured. Recombinant wt αSyn has long been known to exist in a predominantly unstructured "random coil" conformation (8), and both the fPD mutant E46K and the 2K and 3K artificial mutants do not appear to affect the protein secondary structure enough to cause a change in the far-UV CD spectrum (Fig. 1B). Analogously, the weak near-UV CD signal of the protein is minimally affected by the mutations, if at all (Fig. S1). Nevertheless, Size-Exclusion

Chromatography (SEC) analysis of the mutants' hydrodynamic radius shows a marked decrease moving from wt to E46K (as previously reported (32)) and from E46K to 2K and 3K (Fig. 1C). While the elution volumes still indicate that all the mutants have an extended conformation (since their hydrodynamic radii are unusually high for 14.5-kDa proteins (8)), the addition of Ks induces increasingly more compact structures.

Since CD cannot document small changes in the proteins' conformational equilibria upon E-to-K substitution, ^{1}H-^{15}N HSQC spectra of the ^{15}N-labeled proteins in buffer (at 15ºC) were also recorded and compared (Fig. 2A). In accord with the CD data, the overall spread of the amide peaks of the E46K-like mutants reflects their disordered structure. However, numerous shifts in the resonances can be clearly observed and some of these changes (especially in the case of C-terminal residues) correlate well with the increment in E-to-K mutations. After assignment of the amide peaks, relying on deposited datasets of the ^{1}H-^{15}N HSQC of wt αSyn (33, 34), a histogram of the absolute weighted chemical shift perturbations throughout the protein sequence was obtained, highlighting the regions that are mostly affected by the sequential E-to-K substitutions (Fig. 2B). When compared to wt αSyn, all the mutations show changes in the N-terminus, not only around the site of the E-to-K substitutions, but also mild, medium, and long-range effects. Interestingly, the C-terminal region is also markedly affected by the mutations and in a much clearer incremental fashion (i.e. correlating with the insertion of more and more Ks) than the N-terminus. wt αSyn is known to exist in a variety of unstructured conformational states, of which many are stabilized by long-range N-to-C interactions, probably electrostatic in nature (35, 36). E46K αSyn has also been shown, in both experiments and simulations, to have increased long-range contacts, most likely due to the substitution of the E46 negative charge with a positively charged lysine, making transient bonding with the negative C-terminal region more favorable (37, 38). We can imagine similar (and much more marked, at least according to the magnitude of the perturbations) effects playing a role in this case, thus explaining the decrease in hydrodynamic radius as well (Fig. 1C). Indeed, analysis of the charge distribution of the N-terminus of wt αSyn and comparison with its K, 2K and 3K mutants confirms that, while the overall charge density is unperturbed by the mutations, the E-to-K substitutions increase the overall charge polarization (Fig. 2C). If we take the segment 1-95 as the N-terminus of the protein, we observe a net +6 charge increase going from wt αSyn (which has a mild imbalance of +3.1 charges) to 3K αSyn.

E35K and E46K most affect the micelle-bound "broken helix"

Extensive biophysical work has concluded that a single continuous helix is the preferred conformation of αSyn upon interaction with curved lipid bilayers (e.g. Small Unilamellar Vesicles, SUVs; Large Unilamellar Vesicles, LUVs) similar, in morphology and composition, to the physiological membranous interactants of αSyn (17, 39). Nevertheless, the best-characterized helical structure of αSyn is that classically described as a "broken helix" (33), and observed mainly in lipoprotein nanoparticles (12) and on detergent micelles (33, 40). We therefore decided to explore how the E-to-K mutations affected αSyn's "broken helix" structure by recording ^{1}H-^{15}N HSQC spectra of the recombinant ^{15}N-labeled mutants in the presence of SDS micelles (Fig. 3A). The distribution of the amide resonances of all the mutants is consistent with a folded structure, and the E-to-K mutations seem to cause relatively few perturbations in the chemical shifts, which are mainly clustered in the N-terminus of the protein, as is clearest after plotting the chemical shift perturbations of each mutant compared to wt αSyn (Fig. 3B). By comparing each of the "K mutants" with its homolog (with one less E-to-K substitution) we can also probe how each site affects the structure of the "broken helix" (though in an imperfect fashion, as the perturbations could well not be perfectly additive). These differences are shown in Fig. 3C. While both E46K and E35K have robust, long-ranging effects on αSyn's resonances, E61K appears to act prevalently on a local scale, with only minor "ripples" in the residues away from the substitution site. Inspection of the deposited structure of micelle-bound αSyn (PDB: 1XQ8) allows us to draw structural correlations which confirm our NMR findings. While E35 and E46 are localized close to the "ordered loop" region and oriented in a way that facilitates electrostatic interactions with the

negatively charged heads of the detergent, E61 points directly opposite to the hydrophobic side of the second amphipathic helix and can therefore be expected to only affect marginally the structure of αSyn upon charge inversion (Fig. 3C, *inset*). These results contradict previous *in vitro* and *in vivo* work with the E46K-like mutants, which showed a stepwise increase in toxicity with further E-to-K mutations and, if anything, a more prominent effect of the E61K mutation (28, 31). A structure other than the "broken helix" could be predominant in cellular and murine models and would thus explain such inconsistencies.

E-to-K mutations mildly increase the "avidity" for curved membranes

To further explore the molecular events leading to the vesicle clustering and toxicity caused by overexpression of the E46K-like mutants (26), we studied the binding of wt αSyn and its E-to-K mutants to negatively charged Small Unilamellar Vesicles (SUVs). Upon interaction with curved membranes, such as when titrating the recombinant protein with SUVs, αSyn undergoes a coil-to-helix transition which can be monitored by CD (13). SUVs were prepared by sonication (obtaining a dispersion of vesicles ~33 nm in diameter, *see* Table S2) of a 70:30 hydrated mixture of zwitterionic 1-palmitoyl-2-oleoylphosphatidylcholine (POPC) and anionic 1,2-dioleoyl-*sn*-glycero-3-phospho-L-serine (DOPS). αSyn, as expected, bound avidly (Fig. 4A and B) to these membranes; the titration curves obtained were analyzed to derive the thermodynamic and stoichiometric parameters of the binding event. An *N* independent binding sites model was used to describe the binding events (*see* Experimental Procedures). Since the molar lipid concentration was used as the ligand concentration, the *N* value, rather than the number of binding sites, measures the average number of lipid molecules that are necessary to form a lipid binding site for αSyn. As the number of lipid molecules constituting a vesicle can be considered constant, *N* is then inversely proportional to the number of binding sites on a given vesicle. A decrease in *N* therefore reflects a higher number of saturable binding sites on the vesicles' surface and vice versa. We observe a mild decreasing trend in the *N* values obtained by fitting the mutants' titration curves; this represents an increase in the number of αSyn binding sites, although this result does not reach significance in the cases of K and 2K αSyn (Fig. 4C and Table S3). While E46K has been previously reported to have a higher affinity for negatively charged, curved lipid interfaces (41, 42), more recent work has not been able to detect differences with wt αSyn, either when using recombinant E46K αSyn and artificial liposomes or measuring synaptic localization in cultured primary neurons (43). It must also be noted that E61K has the highest effect on *N* among all the E-to-K mutations. Finally, the increase in binding does not correspond to significant changes in the plateau ellipticity values associated with the membrane-bound helical structures, suggesting only minor (if any) conformational rearrangements. Similar CD-monitored lipid-into-protein titrations were also performed in the presence of 150 mM NaCl, in order to test the effect of a higher ionic strength on αSyn's binding behavior, and confirmed the results obtained in low-salt conditions (Fig. S4 and Table S3). As expected, the endpoint ellipticities and the k_Bs are smaller, probably due to the electrostatic masking of the charged moieties in the lipid heads and in some of αSyn's residues, decreasing the strength of ionic interactions at the vesicular interface.

Knowing the critical role of cholesterol-rich lipid rafts in αSyn's physiology (18) and the high content of cholesterol in the membranes of synaptic vesicles (15), we also studied whether the rigidity of the double layer affected the binding of the E-to-K mutants. CD-monitored titrations were performed in the same way as those with 70:30 POPC:DOPS, but a 52.5:17.5:30 POPC:DOPS:cholesterol lipid dispersion was sonicated to generate SUVs (~36 nm in diameter). The results (both *N* and the plateau ellipticity values) are similar to those obtained with POPC:DOPS SUVs (Fig. 5), but in this case there is a much clearer distinction between the binding behavior of the 3K and that of the other mutants, which are practically indistinguishable and show no trends in their *N* values (Fig. 5B). Once again, E61K appears to be the mutation site which most significantly affects the ability of αSyn to associate with membranes.

While CD-monitored lipid-into-protein titrations can provide accurate estimates of the number of lipids per binding site (*N*) and macroscopic structural information on the coil-to-helix

transition, their estimates of the apparent microscopic binding constants (k_B) are poor. For this reason, and to confirm the previous results by means of an independent technique, we also measured the binding curves of wt αSyn and its E-to-K mutants to SUVs by Isothermal Titration Calorimetry (ITC). The results for 70:30 POPC:DOPS are analogous to those found by CD-monitored titrations (Fig. S5A, C and Table S3). In addition to N, ITC provides thermodynamic information on the heat released upon binding (Fig. S5D), but the interpretation of these data, although marked differences are observed between the mutants, is made challenging by the fact that the ΔH values are a combination, among others, of the heat of binding of αSyn to the membranes, the heat exchanged due to the coil-to-helix transition, and the heat contributions of the lipids themselves (e.g. tail hydration, bilayer rearrangement, and remodeling). ITC, as expected, provides much more accurate estimates of the apparent binding constants, which, however, do not appear to change significantly between mutants (Fig. S5E and Table S3). ITC of 52.5:17.5:30 POPC:DOPS:cholesterol SUVs did not detect any binding processes in the cases of wt, K and 2K αSyn, possibly because the heat exchanges of bilayer reorganization processes masked the heat from the protein's binding and folding. The only mutant which showed a clear sigmoidal profile by ITC was 3K αSyn, again in accord with the CD evidence that the E61K mutation alone increases binding to more rigid membranes (Fig. S5B and Table S3).

In conclusion, it is important to consider how, based on the combined CD and ITC data, the αSyn mutants (3K in particular) do not necessarily appear to have a higher "affinity", in its classic interpretation (higher k_B), for curved charged membranes. Rather, the more E-to-K mutations are present, the more αSyn molecules seem to be able to bind to a single vesicle, which, to borrow from the nomenclature of polyvalent interactions, corresponds to a higher "avidity" of lipid bilayers for the E46K-like mutants (44).

E-to-K mutations cause a progressive loss of curvature selectivity

One rarely explored aspect of the molecular pathology of fPD-associated αSyn mutants is how their binding selectivity is affected by mutations. Since αSyn has long been known to bind preferentially to small vesicles (13), and its dynamic association with synaptic vesicles upon exo- and endocytosis is believed to be central to its function (19, 45), we chose to explore how E-to-K mutations modify αSyn's selectivity for certain curvature radii. We performed CD-monitored titrations of wt αSyn and its E-to-K mutants with Large Unilamellar Vesicles (LUVs) prepared by extrusion of a 70:30 POPC:DOPS dispersion using 0.1-μm polycarbonate membranes (obtaining vesicles ~100 nm in diameter, Table S2). As expected, the binding propensity of both wt αSyn and its mutants to charged LUVs is markedly lower than that observed with SUVs (Fig. 6A and B). The curvature of the titration curves is much shallower than the sharp bends of SUVs titrations, signaling that k_Bs are orders of magnitude lower (Table S3). The ellipticities of the helical conformers of LUV-bound αSyn are also roughly half of those recorded before (Fig. 6A and 4A), possibly because of a more dynamic equilibrium between partly folded and partly unfolded conformations, which has been proposed to be one of the curvature-sensing mechanisms adopted by αSyn (46). Furthermore, while the effects of E-to-K mutations are generally mild in the SUV titrations (possibly because of the overall high affinities), robust changes are evident in the LUV titrations, especially after curve fitting with our N independent binding sites model (Fig. 6C and D). Going from wt αSyn to 3K we see a decrease in N (number of lipids per binding site) which is truly stepwise incremental, as are effects observed in cellular models (28). In addition, while we could not detect significant differences between the "avidity" (nor the "affinity") of E46K and wt αSyn using SUVs, here we observe a clear loss of curvature selectivity with the introduction of the fPD-causing mutation, which could be one of the factors underlying its propensity for pathology. In addition to the increased "avidity" of negatively charged LUVs for E46K-like mutants, a slight increase in plateau ellipticities is also detected, but, while significant, the effects are as minor as those previously described in the case of SUVs (Fig. 6D).

As with the SUVs titrations, the experiments were repeated in the presence of 150 mM NaCl to explore the effect of an increased ionic strength (Fig. S6). However, given the already weak

affinity of αSyn for the mildly charged LUVs, the presence of a higher salt concentration almost completely abolished binding for all mutants except 3K (confirming its much stronger ability to bind bilayers in all of the conditions studied). In order to be able to quantitatively compare the different E-to-K mutants, we used the slope of the binding curve in its early phase as a measure of the strength of the affinity (Fig. S6C). Although not as mechanistically valuable as the *N* independent binding site model, the comparison of the binding slopes among the different mutants still shows a much stronger progression (wt to 3K) than the one observed with SUVs (Fig. S6D), confirming previous conclusions.

E46K-like mutants have increasing membrane remodeling abilities

One further aspect of αSyn's interplay with membranes was then studied, namely its ability to remodel lipid bilayers into bilayer tubes, micellar tubes and lipoprotein nanoparticles (12, 47, 48). A dispersion of multilamellar vesicles (MLVs) was prepared by hydration of a 90:10 mixture of 1-palmitoyl-2-oleoyl-*sn*-glycero-3-phospho-(1'-*rac*-glycerol) (16:0-18:1 PG or POPG) and POPC. The content of charged lipids was chosen in order to magnify differences in tubulation rates arising from progressive E-to-K mutations. Upon addition of αSyn, the robust scattering signal from the heterogeneous dispersion of large (d > 1 μm) MLVs is drastically decreased as αSyn induces the formation of tubules, vesicular structures, and lipoprotein nanoparticles, which all exhibit reduced scatter. Remodeling rates can thus be studied by light scattering (e.g. absorbance at 500 nm) and also by CD, since it is the association of αSyn with the vesicles (and its consequent folding) that drives the membrane remodeling (Fig. 7A and B). The rates of vesicle clearance correlate well with αSyn's increasing avidity for LUVs, with a stepwise increase going from wt to 2K αSyn; however, they plateau at 3K, showing little difference upon introduction of E61K. Fitting of the clearance curves using a two-phase exponential decay confirms qualitative observations (the decay rates of the "slow" phase were compared, since the early "fast" phase has too few points to provide accurate parameters). Half-lives decrease upon introduction of the first two E-to-K mutations (E46K and E35K), and no differences can be detected between 2K and 3K (both in absorbance-monitored and CD-monitored experiments, Fig. 7C). Electron micrographs obtained after mixing wt αSyn and its E-to-K mutants with MLVs also reveal robust membrane remodeling in all cases. However, the introduction of successive E-to-K mutations leads to the more frequent appearance of narrower (d ~ 5-6 nm) membrane tubes (Fig. 7D-G). Previous work (47, 48) has shown how such narrow tubes are micellar in nature and are increasingly generated at higher protein-to-lipid ratios. This phenomenon reflects the increased avidity of E-to-K mutants towards large curved membranes (Fig. 6), resulting in a greater number of bound αSyn molecules and more profound bilayer remodeling.

Discussion

In the search for the molecular determinants underlying the inception of PD and other synucleinopathies, a great deal of attention has been devoted to the biophysics and biochemistry of fPD-associated αSyn mutants. Historically, most of these mutants were characterized in their ability to generate toxic oligomers upon aggregation (49, 50). However, after the discovery of the robust and specific lipid-binding ability of wt αSyn (13), several lines of evidence have shown how disruption of such binding equilibria can also lead to cellular toxicity and disease (20, 24, 51).

In this work we have focused our attention on the molecular mechanism behind the lipid-mediated toxicity of E46K αSyn and its exacerbated analogs (2K and 3K αSyn, Fig. 1A), which have been shown, in both cellular and murine models, to cause trafficking defects, αSyn-rich vesicular inclusions and a PD-like motor phenotype (26, 28, 31). We described how E46K, 2K and 3K αSyn, in accord with previous reports (26, 31), exhibit a stepwise increase in membrane avidity (Fig. 4, 5 and 6) and in their membrane-remodeling abilities (Fig. 7). While the effects of E46K and E46K-like mutations on αSyn's binding to small curved vesicles are relatively minor (Fig. 4 and 5), these mutants cause a much more profound disruption in the protein's curvature selectivity, which is almost completely abolished in 3K αSyn (Fig. 6). Although some reports have previously described E46K αSyn as binding more avidly to small,

charged vesicles (41, 42), our tightly controlled CD-monitored titration experiments, combined with an independent technique such as ITC, fail to reproduce these results, in agreement with more recent work (43). 2K and 3K αSyn also display only small (or even undetectable) effects when SUVs are used as their binding partners (Fig. 4 and 5), but exhibit much more severe changes in their LUV-binding ability (Fig. 6), strengthening the case that they behave as exacerbated E46K mutants. Finally, membrane tubulation assays, performed using heterogeneous dispersions of large MLV, confirm such trends (Fig. 7). Successive E-to-K mutations appear to transform αSyn from being predominantly a "curvature sensor" (wt) to acting as a robust "curvature inducer" (2K, 3K), although it is likely that these aspects are ultimately linked and can both be traced back to the loss of curvature selectivity.

We hypothesize that behind the pathogenesis of both E46K-associated fPD and 2K/3K murine models of synucleinopathy there could be a redistribution of the membrane-bound αSyn population to larger intracellular vesicles (such as those involved in secretory or endosomal pathways), rather than an increased avidity for synaptic vesicles, their natural binding partners. Such shift could then act as a combined toxic gain-of-function, with αSyn disrupting the vesicular trafficking through its abnormal binding, and a damaging loss-of-function, due to αSyn being less available at the synaptic bouton where it would normally regulate synaptic vesicle fusion and recycling (6).

In addition to characterizing the molecular pathology of E46K-like mutants, the sequential insertion of E-to-K mutations at specific points in the 11-mer repeat region allows us to rationalize the observed phenomena using structural determinants. αSyn's primary structure, upon inspection of its sequence hydrophobicity (Fig. S7A), is clearly split between a neutral (neither robustly polar nor apolar) N-terminus (1-95) and a negatively charged C-terminus, consistently characterized as disordered. Also, either by plotting Eisenberg's hydrophobic moment (measuring the degree of polarity segregation in a helical structure) vs. the helix's periodicity (52, 53) or by calculating the Fast Fourier Transform of the vector of the side chain hydrophobicities in the segment 1-95 (54, 55) we can see how the N-terminus can be arranged into robustly amphiphilic helical structures with periodicities around 3.6 amino acids per turn (Fig. 8 and S7B). Depending on the amphiphilic interactant, αSyn's membrane-bound (or detergent-bound) structure has been either described as a "broken helix", with two α-helical segments (3.6 amino acids per turn) connected by an ordered loop (33, 40), or as a single continuous 11/3 helix (~3.67 amino acids per turn), spanning throughout the whole 1-95 region (17, 39). Subsequent work has described the possibility of an interchange between these two forms, quantifying the equilibrium as shifted towards the 11/3 helix when αSyn is bound to charged SUVs rather than detergent micelles (12, 56).

If we plot a Schiffer-Edmundson helical wheel diagram (57) with an 11/3 periodicity and its helical net (58), spanning αSyn's N-terminal region (1-95), and highlight the positions of the three Glu residues progressively substituted by lysines, we can hypothesize how their arrangement could increase their avidity for bilayers with a progression comparable to that observed in our experiments (Fig. S8). The proximity of E35, 46 and 61 to the negatively charged surface of the vesicle's membrane could allow the formation of ionic bridges between the positively charged lysines and the phosphate heads, thus favoring the binding and stabilizing the 11/3 helix. Although all three residues are in very similar positions, the presence of the 53-56 (ATVA, Fig. 1A) break in the 11-mer periodicity region shifts E61 slightly closer to the membrane surface. While this small difference might be masked in 3K αSyn by the dynamic nature of the 11/3 helix (17, 46, 59), especially in fluid DOPC/DOPS SUVs (Fig. 4), it could become more important in the case of rigid membranes, rich in cholesterol, thus also explaining the lone increased avidity of 3K for such interfaces (Fig. 5).

In conclusion, our biophysical characterization recapitulates all the relevant features of cellular and murine models of the E46K-like mutants, and, at the same time, allows us to advance the possibility of a loss of curvature selectivity, rather than increased membrane affinity, as the critical dyshomeostasis in synucleinopathies. In light of these results, there appears to be an even greater translational potential in therapies modulating the cellular lipid composition in order to compensate

for αSyn defects, which has recently started being explored (60, 61).

Experimental Procedures

Materials — 1-palmitoyl-2-oleoyl-glycero-3-phosphocholine (16:0-18:1 PC or POPC), 1,2-dioleoyl-*sn*-glycero-3-phospho-L-serine (18:1 PS or DOPS), and 1-palmitoyl-2-oleoyl-*sn*-glycero-3-phospho-(1'-*rac*-glycerol) (16:0-18:1 PG or POPG) were purchased from Avanti Polar Lipids (Alabaster, AL) as chloroform solutions. All other chemicals were obtained from Sigma-Aldrich (St. Louis, MO) unless otherwise noted.

Molecular Cloning — pET21a-alpha-synuclein, encoding codon-optimized untagged human αSyn, was a gift from the Michael J. Fox Foundation MJFF (Addgene plasmid # 51486). Fragments encoding E46K ('K'), E35,46K ('2K') and E35,46,61K ('3K') αSyn were amplified with PfuUltra II Fusion HS (Agilent Technologies, Santa Clara, CA) using their constructs in pcDNA4 (28) as templates and the primers αSyn_InFu_FWD 5'-AAGGAGATATACATATGGATGTATTCATG AAAGGACTTTCAAAGG-3' and αSyn_InFu_REV 5'-TGCTCGAGTGCGGCCGCTCAGGCTTCAGGT TCGTAGTCTTGATACC-3'. The amplified fragments were then inserted into pET21a (linearized with NdeI/NotI) using the In-Fusion HD Cloning Kit (Takara Bio, Mountain View, CA), following the manufacturer's protocol. Cloning of pET21a-K-αSyn, -2K-αSyn, -3K-αSyn was confirmed by DNA sequencing and restriction analysis.

Protein Expression and Purification — BL21(DE3) *E. coli*. (New England Biolabs, Ipswich, MA) were transformed with the pET21a-based constructs and single colonies inoculated in LB+ampicillin. Cultures were induced at an OD_{600} of ~0.5 with 1 mM isopropyl-β-D-thiogalactopyranoside (IPTG) for 4 hrs. The cell pellet, after harvesting, was resuspended in 20 mM Tris buffer, 25 mM NaCl, pH 8.00, and lysed by boiling for 15 min. The supernatant of a 20-min., 20,000*xg* spin of the lysate was then further processed. The sample was loaded on two 5-mL (tandem) HiTrap Q HP anion exchange columns (GE Healthcare, Pittsburgh, PA), equilibrated with 20 mM Tris buffer, 25 mM NaCl, pH 8.00. αSyn was eluted from the columns with a 25-1000 mM NaCl gradient of 20 mM Tris buffer, 1 M NaCl, pH 8.00. Peak fractions were pooled and further purified via gel filtration on a HiPrep Sephacryl S-200 HR 16/60 gel filtration column (GE Healthcare, Pittsburgh, PA) using 50 mM NH_4Ac, pH 7.40 as running buffer. Peak fractions (>95% pure, by Coomassie Brilliant Blue-stained SDS-PAGE) were pooled, aliquoted, lyophilized and stored at -20ºC. Purified samples were also analyzed by Matrix-Assisted Laser Desorption Ionization-Time Of Flight (MALDI-TOF) Mass Spectrometry (MS) and trypsin digestion followed by MALDI-TOF MS, to confirm the intact mass and sequence of the proteins (Molecular Biology Core Facilities, Dana-Farber Cancer Institute). Lyophilized proteins were reconstituted fresh, before experiments, in 10 mM NH_4Ac, pH 7.40, and not reused (re-lyophilized and reconstituted) more than twice. Protein solutions were spun down every time after resuspension, before spectroscopic quantitation of the protein concentration, at 21,130*xg* for 20 min. at 4ºC, in order to remove any large αSyn aggregates. Concentration was quantified by measuring the absorbance at 280 nm (ε=0.412 $mg \cdot mL^{-1} \cdot cm^{-1}$).

^{15}N-Labeled Protein Expression — For the expression of ^{15}N-labeled αSyn, the bacteria were grown in M9 complete medium+ampicillin, supplemented with $^{15}NH_4Cl$. M9 complete medium was prepared fresh from a 10x M9 medium stock (60 $g \cdot L^{-1}$ Na_2HPO_4, 30 $g \cdot L^{-1}$ KH_2PO_4, 5 $g \cdot L^{-1}$ NaCl), 50x 20% D-glucose, 1000x 1 M $MgSO_4$, 5000x 1 M $CaCl_2$, 1000x 1 $mg \cdot mL^{-1}$ thiamine and biotin, 100x trace element solution, 1000x vitamin solution and 1 $g \cdot L^{-1}$ $^{15}NH_4Cl$. The 100x trace element solution was prepared by dissolving (in 1 L MilliQ water) 5 g ethylenediaminetetraacetic acid (EDTA), 0.50 g $FeCl_3$, 84 mg $ZnCl_2$, 12 mg $CuSO_4$, 10 mg $CoCl_2 \cdot 6H_2O$, 10 mg H_3BO_3, 1.6 mg $MnCl_2 \cdot 4H_2O$, 1.6 mg $Na_2MoO_4 \cdot 2H_2O$, and adjusting the pH to 7.0 (it was then filter-sterilized and stored at RT). The 1000x vitamin solution was prepared by dissolving (in 1 L 95% MilliQ water, 5% acetonitrile), 50 mg riboflavin, 0.5 g niacinamide, 0.5 g pyridoxine hydrochloride, 0.5 g thiamine. After filtration with a 0.22-µm cutoff (to sterilize and remove the

undissolved riboflavin), the solution was stored at 4ºC, protected from light. BL21(DE3) *E. coli*. (New England Biolabs, Ipswich, MA) were transformed with the pET21a-based constructs and single colonies inoculated in 2xYT+ampicillin. Cultures were grown for 6-8 hrs. at 37ºC under shaking, then used to inoculate an overnight pre-culture in M9 complete medium+ampicillin, which, on the following day, was diluted again 1:10 in M9 complete medium+ampicillin. The expression and purification of ^{15}N-labeled proteins were, from this point on, performed as described under *'αSyn Expression and Purification'*.

Size-Exclusion Chromatography (SEC) — Samples were injected on a Superdex 200 (10/300 GL) column (GE Healthcare, Pittsburgh, PA) at RT and eluted with 50 mM NH_4Ac, pH 7.40, while measuring (in-line) the conductivity and the 280-nm absorption of the eluate. For size estimation, a gel filtration standard (Catalog #151-1901, Bio-Rad, Hercules, CA) was run on the column, and the calibration curve was obtained by semi-logarithmic plotting of molecular weight versus the elution volume divided by the void volume.

Liposome Preparation — Aliquots from chloroform stock solutions of POPC, DOPS and cholesterol were mixed thoroughly in the desired proportions and dried under a stream of argon. The dried lipid film was then kept under vacuum overnight, to remove traces of organic solvent. For both Small and Large Unilamellar Vesicles (SUVs and LUVs), lipid solutions were prepared fresh by resuspending the dried lipids in 10 mM NH_4Ac, pH 7.40, to their final concentrations and hydrating them for 1 h at 37ºC, while nutating. SUVs were prepared by pulse-sonicating the phospholipid suspensions for 10-20 min. at RT with a microtip sonicator (Misonix S-4000, Qsonica, Newtown, CT). The SUVs suspensions were then spun down at 21,130*xg* for 10 min. to remove any metal particles and larger lipid aggregates. LUVs were prepared by manual extrusion (25 passes), using an Avanti Mini-Extruder (Avanti Polar Lipids, Alabaster, AL) and 0.1-μm polycarbonate membranes, following the manufacturer's protocol. For Multilamellar Vesicles (MLVs), aliquots from the lipids' stock solutions in chloroform were mixed thoroughly in the desired proportions and dried under a stream of nitrogen. The dried lipid film was then kept under vacuum for >12 hrs., to remove traces of organic solvent. MLV dispersions were prepared by resuspending the dried lipids in the buffer of choice and vortexing.

Circular Dichroism (CD) — Spectra were recorded with a Jasco J-815 spectropolarimeter (Jasco, Easton, MD) at 25ºC, using a 1-mm pathlength cuvette for far-UV CD (a 1-cm pathlength cuvette was used for near-UV CD measurements). Temperature control with an accuracy of ±0.1ºC was achieved with a heating/cooling accessory equipped with a Peltier element (PFD-425S) connected to a water thermostatic bath. When possible, buffer spectra were recorded and subtracted. In titration experiments, spectra were corrected for the dilution effect from the addition of titrant; control lipid-into-buffer titrations were also recorded to confirm the negligibility of the liposome scattering signal. Three independent titrations (although with the same vesicle preparation) were performed for each condition. In "high-salt" (150 mM NaCl) titrations, NaCl was spiked into protein and lipid samples right before the experiments, using a 5 M stock.

Stoichiometric and thermodynamic parameters (N, $[\Theta]^{222}_{helix}$, k_B) were determined by fitting the CD titration curves according to an N independent binding sites model. The expression of the fractional saturation ϑ (ratio of occupied sites to total sites) as a function of P_t and L_t (the total concentrations of protein and lipid), k_B (the apparent microscopic binding constant), and N (the number of saturable binding sites on the surface of the vesicles) was taken from the classic derivation of the Wiseman isotherm for an N independent binding sites model (62):

$$\vartheta = \frac{1}{2}\left[1 + \frac{L_t}{NP_t} + \frac{1}{Nk_BP_t} - \sqrt{\left(1 + \frac{L_t}{NP_t} + \frac{1}{Nk_BP_t}\right)^2 - \frac{4L_t}{NP_t}}\right] \quad (1)$$

In CD-monitored titrations the 222-nm signal comes from the combination of the random coil signal from unbound αSyn and the helical signal of lipid-bound αSyn, each proportional to the molar ratios of the two species ($[\Theta]_i^{222}$ is the molar, or residue, ellipticity at each point of the titration):

$$[\Theta]_i^{222} = \frac{[PL_n]}{P_t}[\Theta]_{helix}^{222} + \frac{[P]}{P_t}[\Theta]_{coil}^{222} \quad (2)$$

ϑ (at each point of the titration) can then be expressed as:

$$\frac{[PL_n]}{P_t} = \vartheta = \frac{[\Theta]_i^{222} - [\Theta]_{coil}^{222}}{[\Theta]_{helix}^{222} - [\Theta]_{coil}^{222}} \quad (3)$$

Combining (1) and (3) we can write $[\Theta]_i^{222}$ as a function of the lipid:protein molar ratio X, obtaining the final form of the fitting equation:

$$[\Theta]_i^{222} = [\Theta]_{coil}^{222} + \frac{[\Theta]_{helix}^{222} - [\Theta]_{coil}^{222}}{2}\left[1 + \frac{X}{N} + \frac{1}{Nk_BP_t} - \sqrt{\left(1 + \frac{X}{N} + \frac{1}{Nk_BP_t}\right)^2 - \frac{4X}{N}}\right]$$

Since the molar lipid concentration in the cuvette is used as L_t, the N value, rather than the number of binding sites, measures the average number of lipid molecules forming one lipid binding site.

Isothermal Titration Calorimetry (ITC) — ITC measurements were performed on an iTC200 instrument (Malvern Instruments, Westborough, MA). Typically, 18 fresh SUVs dispersion injections of 2 µL each (+1 0.4 µl pre-injection) were titrated in the calorimeter chamber. Both linear baselines and control titrations of vesicles into buffer alone were used for baseline subtraction. The data were processed using the MicroCal ORIGIN 7.0 software (Malvern Instruments; OriginLab, Northampton, MA, USA). After integration of the differential power signal, stoichiometric and thermodynamic parameters (N, ΔH, k_B) were determined by fitting the sigmoidal titration curve using an N independent binding sites model (with the sites assumed to localize on the vesicles' outer surface). The apparent (given the approximations used) microscopic binding constant was labeled k_B. The total lipid concentration in the syringe was taken as the ligand concentration; thus, the N value measures the average number of lipid molecules forming a binding site. In all experiments the stoichiometric and thermodynamic parameters were obtained from three independent titrations (though performed using the same vesicle preparation). ΔS was obtained from $\Delta G = -RTlnk_B$ and ΔH.

Dynamic Light Scattering (DLS) — The hydrodynamic radius of the liposomes (5 mM) was measured using a DynaPro dynamic light scattering instrument (Wyatt Technology Corporation, Santa Barbara, CA). The DLS cell was thermostated at 20.0ºC; the hydrodynamic radii were obtained by averaging three independent samples.

Phospholipid Vesicle Clearance Assay — The ability of αSyn and its mutants to remodel phospholipid vesicles was studied by measuring light scattering as a function of time using a Jasco V-550 UV/VIS spectrophotometer (Jasco, Easton, MD), as previously described (47). Briefly, light scattering was monitored at 500 nm, using a 2-nm slit width and a "Medium" response time. MLVs were prepared in 20 mM HEPES, 100 mM NaCl, pH 7.40. No changes in the light scattering of the MLV dispersion were observed in the absence of

protein. CD-monitored vesicle clearance experiments were performed at 25ºC, using a Jasco J-810 spectropolarimeter (Jasco, Easton, MD), in a 1-mm quartz cell. Blanks were recorded under similar conditions and subtracted.

Transmission Electron Microscopy (TEM) — TEM specimens were prepared on carbon-coated Formvar grids (Electron Microscopy Sciences, Hatfield, PA). Samples were adsorbed on the grids for 5 min., then negatively-stained with 1% (w/v) aqueous uranyl acetate. Images were taken on a JEOL 1400 transmission electron microscope (JEOL USA Inc., Peabody, MA) at an accelerating voltage of 100 kV.

NMR — ^{1}H-^{15}N HSQC spectra of ^{15}N-labeled αSyn were recorded in 50 mM phosphate buffer, pH 6.80, 10% D_2O. Spectra were recorded on a 600 MHz Bruker AVANCE II spectrometer (Bruker, Billerica, MA) equipped with a Prodigy CryoProbe, at either 15ºC (120 µM αSyn) or 37ºC (120 µM αSyn + 15 mM SDS). Resonances were assigned, where possible, by inspection and comparison with the previously assigned spectra of wt αSyn (BMRB 5744, 6968) (33, 34). Data processing and analysis were performed with the Bruker TopSpin software and CcpNmr Analysis (63). Perturbations in the chemical shift values for ^{1}H and ^{15}N were calculated as $[(\Delta\delta^{1}H)^{2}+(0.15\cdot\Delta\delta^{15}N)^{2}]^{1/2}$.

Data Analysis and Primary Sequence Analysis — Data analysis was performed using GraphPad Prism 7 (GraphPad Software, La Jolla, CA, USA). Statistical significance was determined by ordinary one-way ANOVA followed by Sidak's multiple comparisons test, with a single pooled variance; n.s. $p>0.05$, * $p\leq0.05$, ** $p\leq0.01$, *** $p\leq0.001$, **** $p\leq0.0001$.
Primary sequence analyses were performed with Microsoft Excel (Microsoft, Redmond, WA) and Wolfram Mathematica 10 (Wolfram Research, Champaign, IL), using the hydropathy index values of Kyte and Doolittle (64). Helical wheel and net diagrams were plotted using in-house Python code, modeled after the WHEEL and HELNET programs (65).

Acknowledgements.

We thank Kelly Arnett and the Center for Macromolecular Interactions at the Harvard Medical School Department of Biological Chemistry and Molecular Pharmacology for assistance with CD and ITC measurements and many helpful discussions; Simon Jenni, Yoana Dimitrova and the Harrison laboratory at the Harvard Medical School Department of Biological Chemistry and Molecular Pharmacology for the use of instruments and assistance with DLS measurements; Jim Lee and the Molecular Biology Core Facilities of the Dana-Farber Cancer Institute for assistance with mass spectrometry. Finally, we also thank our colleagues at the Ann Romney Center for Neurologic Diseases for many helpful discussions and Martina Astrid Rodda for editing and revising the manuscript.

Conflict of interest.

The authors declare that they have no conflicts of interest with the contents of this article.

References

1. Poewe, W., Seppi, K., Tanner, C. M., Halliday, G. M., Brundin, P., Volkmann, J., Schrag, A.-E., and Lang, A. E. (2017) Parkinson disease. *Nat. Rev. Dis. Prim.* **3**, 17013
2. de Lau, L. M. L., and Breteler, M. M. B. (2006) Epidemiology of Parkinson's disease. *Lancet. Neurol.* **5**, 525–35
3. Iwai, A., Masliah, E., Yoshimoto, M., Ge, N., Flanagan, L., de Silva, H. A., Kittel, A., and Saitoh, T. (1995) The precursor protein of non-A beta component of Alzheimer's disease amyloid is a presynaptic protein of the central nervous system. *Neuron*. **14**, 467–75
4. Shulman, J. M., De Jager, P. L., and Feany, M. B. (2011) Parkinson's disease: genetics and pathogenesis. *Annu. Rev. Pathol.* **6**, 193–222
5. Bendor, J. T., Logan, T. P., and Edwards, R. H. (2013) The function of α-synuclein. *Neuron*. **79**, 1044–66
6. Lautenschläger, J., Kaminski, C. F., and Kaminski Schierle, G. S. (2017) α-Synuclein - Regulator of Exocytosis, Endocytosis, or Both? *Trends Cell Biol.* **27**, 468–479
7. Grace, A. A., and Bunney, B. S. (1984) The control of firing pattern in nigral dopamine neurons: burst firing. *J. Neurosci.* **4**, 2877–90
8. Weinreb, P. H., Zhen, W., Poon, A. W., Conway, K. A., and Lansbury, P. T. (1996) NACP, a protein implicated in Alzheimer's disease and learning, is natively unfolded. *Biochemistry*. **35**, 13709–15
9. Nielsen, J. T., and Mulder, F. A. A. (2016) There is Diversity in Disorder-"In all Chaos there is a Cosmos, in all Disorder a Secret Order". *Front. Mol. Biosci.* **3**, 4
10. George, J. M., Jin, H., Woods, W. S., and Clayton, D. F. (1995) Characterization of a novel protein regulated during the critical period for song learning in the zebra finch. *Neuron*. **15**, 361–72
11. Bussell, R., and Eliezer, D. (2003) A structural and functional role for 11-mer repeats in alpha-synuclein and other exchangeable lipid binding proteins. *J. Mol. Biol.* **329**, 763–78
12. Varkey, J., Mizuno, N., Hegde, B. G., Cheng, N., Steven, A. C., and Langen, R. (2013) α-Synuclein oligomers with broken helical conformation form lipoprotein nanoparticles. *J. Biol. Chem.* **288**, 17620–30
13. Davidson, W. S., Jonas, A., Clayton, D. F., and George, J. M. (1998) Stabilization of alpha-synuclein secondary structure upon binding to synthetic membranes. *J. Biol. Chem.* **273**, 9443–9
14. Eliezer, D., Kutluay, E., Bussell, R., and Browne, G. (2001) Conformational properties of alpha-synuclein in its free and lipid-associated states. *J. Mol. Biol.* **307**, 1061–73
15. Takamori, S., Holt, M., Stenius, K., Lemke, E. A., Grønborg, M., Riedel, D., Urlaub, H., Schenck, S., Brügger, B., Ringler, P., Müller, S. A., Rammner, B., Gräter, F., Hub, J. S., De Groot, B. L., Mieskes, G., Moriyama, Y., Klingauf, J., Grubmüller, H., Heuser, J., Wieland, F., and Jahn, R. (2006) Molecular anatomy of a trafficking organelle. *Cell*. **127**, 831–46
16. Pranke, I. M., Morello, V., Bigay, J., Gibson, K., Verbavatz, J.-M., Antonny, B., and Jackson, C. L. (2011) α-Synuclein and ALPS motifs are membrane curvature sensors whose contrasting chemistry mediates selective vesicle binding. *J. Cell Biol.* **194**, 89–103
17. Jao, C. C., Hegde, B. G., Chen, J., Haworth, I. S., and Langen, R. (2008) Structure of membrane-bound alpha-synuclein from site-directed spin labeling and computational refinement. *Proc. Natl. Acad. Sci. U. S. A.* **105**, 19666–71
18. Fortin, D. L., Troyer, M. D., Nakamura, K., Kubo, S., Anthony, M. D., and Edwards, R. H. (2004) Lipid rafts mediate the synaptic localization of alpha-synuclein. *J. Neurosci.* **24**, 6715–23
19. Fortin, D. L., Nemani, V. M., Voglmaier, S. M., Anthony, M. D., Ryan, T. A., and Edwards, R. H. (2005) Neural activity controls the synaptic accumulation of alpha-synuclein. *J. Neurosci.* **25**, 10913–21
20. Auluck, P. K., Caraveo, G., and Lindquist, S. (2010) α-Synuclein: membrane interactions and toxicity in Parkinson's disease. *Annu. Rev. Cell Dev. Biol.* **26**, 211–33

21. Cooper, A. A., Gitler, A. D., Cashikar, A., Haynes, C. M., Hill, K. J., Bhullar, B., Liu, K., Xu, K., Strathearn, K. E., Liu, F., Cao, S., Caldwell, K. A., Caldwell, G. A., Marsischky, G., Kolodner, R. D., Labaer, J., Rochet, J.-C., Bonini, N. M., and Lindquist, S. (2006) Alpha-synuclein blocks ER-Golgi traffic and Rab1 rescues neuron loss in Parkinson's models. *Science*. **313**, 324–8
22. Gitler, A. D., Bevis, B. J., Shorter, J., Strathearn, K. E., Hamamichi, S., Su, L. J., Caldwell, K. A., Caldwell, G. A., Rochet, J.-C., McCaffery, J. M., Barlowe, C., and Lindquist, S. (2008) The Parkinson's disease protein alpha-synuclein disrupts cellular Rab homeostasis. *Proc. Natl. Acad. Sci. U. S. A.* **105**, 145–50
23. Thayanidhi, N., Helm, J. R., Nycz, D. C., Bentley, M., Liang, Y., and Hay, J. C. (2010) Alpha-synuclein delays endoplasmic reticulum (ER)-to-Golgi transport in mammalian cells by antagonizing ER/Golgi SNAREs. *Mol. Biol. Cell*. **21**, 1850–63
24. Shahmoradian, S. H., Lewis, A. J., Genoud, C., Graff-Meyer, A., Hench, J., Moors, T., Schweighauser, G., Wang, J., Goldie, K. N., Suetterlin, R., Castano-Diez, D., Perez-Navarro, P., Huisman, E., Ipsen, S., Ingrassia, A., Gier, Y. de, Rozemuller, A. J. M., Paepe, A. Da, Erny, J., Staempfli, A., Hoernschemeyer, J., Grosserueschkamp, F., Niedieker, D., El-Mashtoly, S. F., Quadri, M., IJcken, W. F. J. van, Bonifati, V., Gerwert, K., Bohrmann, B., Frank, S., Britschgi, M., Stahlberg, H., Berg, W. van de, and Lauer, M. E. (2018) Lewy pathology in Parkinson's disease consists of a crowded organellar, membranous medley. *bioRxiv*. 10.1101/137976
25. Dettmer, U., Newman, A. J., von Saucken, V. E., Bartels, T., and Selkoe, D. (2015) KTKEGV repeat motifs are key mediators of normal α-synuclein tetramerization: Their mutation causes excess monomers and neurotoxicity. *Proc. Natl. Acad. Sci. U. S. A.* **112**, 9596–601
26. Dettmer, U., Ramalingam, N., von Saucken, V. E., Kim, T.-E., Newman, A. J., Terry-Kantor, E., Nuber, S., Ericsson, M., Fanning, S., Bartels, T., Lindquist, S., Levy, O. A., and Selkoe, D. (2017) Loss of native α-synuclein multimerization by strategically mutating its amphipathic helix causes abnormal vesicle interactions in neuronal cells. *Hum. Mol. Genet.* **26**, 3466–3481
27. Zarranz, J. J., Alegre, J., Gómez-Esteban, J. C., Lezcano, E., Ros, R., Ampuero, I., Vidal, L., Hoenicka, J., Rodriguez, O., Atarés, B., Llorens, V., Gomez Tortosa, E., del Ser, T., Muñoz, D. G., and de Yebenes, J. G. (2004) The new mutation, E46K, of alpha-synuclein causes Parkinson and Lewy body dementia. *Ann. Neurol.* **55**, 164–73
28. Dettmer, U., Newman, A. J., Soldner, F., Luth, E. S., Kim, N. C., von Saucken, V. E., Sanderson, J. B., Jaenisch, R., Bartels, T., and Selkoe, D. (2015) Parkinson-causing α-synuclein missense mutations shift native tetramers to monomers as a mechanism for disease initiation. *Nat. Commun.* **6**, 7314
29. Bartels, T., Choi, J. G., and Selkoe, D. J. (2011) α-Synuclein occurs physiologically as a helically folded tetramer that resists aggregation. *Nature*. **477**, 107–10
30. Dettmer, U., Selkoe, D., and Bartels, T. (2016) New insights into cellular α-synuclein homeostasis in health and disease. *Curr. Opin. Neurobiol.* **36**, 15–22
31. Nuber, S., Rajsombath, M., Minakaki, G., Winkler, J., Müller, C. P., Ericsson, M., Caldarone, B., Dettmer, U., and Selkoe, D. J. (2018) Abrogating Native α-Synuclein Tetramers in Mice Causes a L-DOPA-Responsive Motor Syndrome Closely Resembling Parkinson's Disease. *Neuron*. **100**, 75–90.e5
32. Fredenburg, R. A., Rospigliosi, C., Meray, R. K., Kessler, J. C., Lashuel, H. A., Eliezer, D., and Lansbury, P. T. (2007) The impact of the E46K mutation on the properties of alpha-synuclein in its monomeric and oligomeric states. *Biochemistry*. **46**, 7107–18
33. Chandra, S., Chen, X., Rizo, J., Jahn, R., and Südhof, T. C. (2003) A broken alpha-helix in folded alpha-Synuclein. *J. Biol. Chem.* **278**, 15313–8
34. Bermel, W., Bertini, I., Felli, I. C., Lee, Y.-M., Luchinat, C., and Pierattelli, R. (2006) Protonless NMR experiments for sequence-specific assignment of backbone nuclei in unfolded proteins. *J. Am. Chem. Soc.* **128**, 3918–9
35. Bertoncini, C. W., Jung, Y.-S., Fernandez, C. O., Hoyer, W., Griesinger, C., Jovin, T. M., and Zweckstetter, M. (2005) Release of long-range tertiary interactions potentiates aggregation of

natively unstructured alpha-synuclein. *Proc. Natl. Acad. Sci. U. S. A.* **102**, 1430–5
36. Croke, R. L., Sallum, C. O., Watson, E., Watt, E. D., and Alexandrescu, A. T. (2008) Hydrogen exchange of monomeric alpha-synuclein shows unfolded structure persists at physiological temperature and is independent of molecular crowding in Escherichia coli. *Protein Sci.* **17**, 1434–45
37. Rospigliosi, C. C., McClendon, S., Schmid, A. W., Ramlall, T. F., Barré, P., Lashuel, H. A., and Eliezer, D. (2009) E46K Parkinson's-linked mutation enhances C-terminal-to-N-terminal contacts in alpha-synuclein. *J. Mol. Biol.* **388**, 1022–32
38. Wise-Scira, O., Dunn, A., Aloglu, A. K., Sakallioglu, I. T., and Coskuner, O. (2013) Structures of the E46K mutant-type α-synuclein protein and impact of E46K mutation on the structures of the wild-type α-synuclein protein. *ACS Chem. Neurosci.* **4**, 498–508
39. Jao, C. C., Der-Sarkissian, A., Chen, J., and Langen, R. (2004) Structure of membrane-bound alpha-synuclein studied by site-directed spin labeling. *Proc. Natl. Acad. Sci. U. S. A.* **101**, 8331–6
40. Ulmer, T. S., Bax, A., Cole, N. B., and Nussbaum, R. L. (2005) Structure and dynamics of micelle-bound human alpha-synuclein. *J. Biol. Chem.* **280**, 9595–603
41. Choi, W., Zibaee, S., Jakes, R., Serpell, L. C., Davletov, B., Crowther, R. A., and Goedert, M. (2004) Mutation E46K increases phospholipid binding and assembly into filaments of human alpha-synuclein. *FEBS Lett.* **576**, 363–8
42. Bodner, C. R., Maltsev, A. S., Dobson, C. M., and Bax, A. (2010) Differential phospholipid binding of alpha-synuclein variants implicated in Parkinson's disease revealed by solution NMR spectroscopy. *Biochemistry*. **49**, 862–71
43. Burré, J., Sharma, M., and Südhof, T. C. (2012) Systematic mutagenesis of α-synuclein reveals distinct sequence requirements for physiological and pathological activities. *J. Neurosci.* **32**, 15227–42
44. Mammen, M., Choi, S.-K., and Whitesides, G. M. (1998) Polyvalent Interactions in Biological Systems: Implications for Design and Use of Multivalent Ligands and Inhibitors. *Angew. Chem. Int. Ed. Engl.* **37**, 2754–2794
45. Bartels, T., Ahlstrom, L. S., Leftin, A., Kamp, F., Haass, C., Brown, M. F., and Beyer, K. (2010) The N-terminus of the intrinsically disordered protein α-synuclein triggers membrane binding and helix folding. *Biophys. J.* **99**, 2116–24
46. Fusco, G., De Simone, A., Gopinath, T., Vostrikov, V., Vendruscolo, M., Dobson, C. M., and Veglia, G. (2014) Direct observation of the three regions in α-synuclein that determine its membrane-bound behaviour. *Nat. Commun.* **5**, 3827
47. Varkey, J., Isas, J. M., Mizuno, N., Jensen, M. B., Bhatia, V. K., Jao, C. C., Petrlova, J., Voss, J. C., Stamou, D. G., Steven, A. C., and Langen, R. (2010) Membrane curvature induction and tubulation are common features of synucleins and apolipoproteins. *J. Biol. Chem.* **285**, 32486–93
48. Mizuno, N., Varkey, J., Kegulian, N. C., Hegde, B. G., Cheng, N., Langen, R., and Steven, A. C. (2012) Remodeling of lipid vesicles into cylindrical micelles by α-synuclein in an extended α-helical conformation. *J. Biol. Chem.* **287**, 29301–11
49. Conway, K. A., Lee, S. J., Rochet, J. C., Ding, T. T., Williamson, R. E., and Lansbury, P. T. (2000) Acceleration of oligomerization, not fibrillization, is a shared property of both alpha-synuclein mutations linked to early-onset Parkinson's disease: implications for pathogenesis and therapy. *Proc. Natl. Acad. Sci. U. S. A.* **97**, 571–6
50. Lashuel, H. A., Petre, B. M., Wall, J., Simon, M., Nowak, R. J., Walz, T., and Lansbury, P. T. (2002) Alpha-synuclein, especially the Parkinson's disease-associated mutants, forms pore-like annular and tubular protofibrils. *J. Mol. Biol.* **322**, 1089–102
51. Dettmer, U. (2018) Rationally Designed Variants of α-Synuclein Illuminate Its in vivo Structural Properties in Health and Disease. *Front. Neurosci.* **12**, 1–14
52. Eisenberg, D., Weiss, R. M., and Terwilliger, T. C. (1982) The helical hydrophobic moment: a measure of the amphiphilicity of a helix. *Nature*. **299**, 371–4
53. Eisenberg, D., Weiss, R. M., and Terwilliger, T. C. (1984) The hydrophobic moment detects

periodicity in protein hydrophobicity. *Proc. Natl. Acad. Sci. U. S. A.* **81**, 140–4
54. McLachlan, A. D., and Stewart, M. (1976) The 14-fold periodicity in alpha-tropomyosin and the interaction with actin. *J. Mol. Biol.* **103**, 271–98
55. Finer-Moore, J., and Stroud, R. M. (1984) Amphipathic analysis and possible formation of the ion channel in an acetylcholine receptor. *Proc. Natl. Acad. Sci. U. S. A.* **81**, 155–9
56. Lokappa, S. B., and Ulmer, T. S. (2011) Alpha-synuclein populates both elongated and broken helix states on small unilamellar vesicles. *J. Biol. Chem.* **286**, 21450–7
57. Schiffer, M., and Edmundson, A. B. (1967) Use of helical wheels to represent the structures of proteins and to identify segments with helical potential. *Biophys. J.* **7**, 121–35
58. Lim, V. I. (1978) Polypeptide chain folding through a highly helical intermediate as a general principle of globular protein structure formation. *FEBS Lett.* **89**, 10–4
59. Jiang, Z., Hess, S. K., Heinrich, F., and Lee, J. C. (2015) Molecular Details of α-Synuclein Membrane Association Revealed by Neutrons and Photons. *J. Phys. Chem. B*. **119**, 4812–4823
60. Fanning, S., Haque, A., Imberdis, T., Baru, V., Barrasa, M. I., Nuber, S., Termine, D., Ramalingam, N., Ho, G. P. H., Noble, T., Sandoe, J., Lou, Y., Landgraf, D., Freyzon, Y., Newby, G., Soldner, F., Terry-Kantor, E., Kim, T.-E., Hofbauer, H. F., Becuwe, M., Jaenisch, R., Pincus, D., Clish, C. B., Walther, T. C., Farese, R. V., Srinivasan, S., Welte, M. A., Kohlwein, S. D., Dettmer, U., Lindquist, S., and Selkoe, D. (2018) Lipidomic Analysis of α-Synuclein Neurotoxicity Identifies Stearoyl CoA Desaturase as a Target for Parkinson Treatment. *Mol. Cell*. 10.1016/j.molcel.2018.11.028
61. Vincent, B. M., Tardiff, D. F., Piotrowski, J. S., Aron, R., Lucas, M. C., Chung, C. Y., Bacherman, H., Chen, Y., Pires, M., Subramaniam, R., Doshi, D. B., Sadlish, H., Raja, W. K., Solís, E. J., Khurana, V., Le Bourdonnec, B., Scannevin, R. H., and Rhodes, K. J. (2018) Inhibiting Stearoyl-CoA Desaturase Ameliorates α-Synuclein Cytotoxicity. *Cell Rep.* **25**, 2742–2754.e31
62. Indyk, L., and Fisher, H. F. (1998) Theoretical aspects of isothermal titration calorimetry. *Methods Enzymol.* **295**, 350–64
63. Vranken, W. F., Boucher, W., Stevens, T. J., Fogh, R. H., Pajon, A., Llinas, M., Ulrich, E. L., Markley, J. L., Ionides, J., and Laue, E. D. (2005) The CCPN data model for NMR spectroscopy: development of a software pipeline. *Proteins*. **59**, 687–96
64. Kyte, J., and Doolittle, R. F. (1982) A simple method for displaying the hydropathic character of a protein. *J. Mol. Biol.* **157**, 105–32
65. Jones, M. K., Anantharamaiah, G. M., and Segrest, J. P. (1992) Computer programs to identify and classify amphipathic alpha helical domains. *J. Lipid Res.* **33**, 287–96

FOOTNOTES

The abbreviations used are: Parkinson's Disease, PD; autosomal dominant Parkinson's Disease (familial PD), fPD; 1-palmitoyl-2-oleoyl-glycero-3-phosphocholine, POPC; 1,2-dioleoyl-*sn*-glycero-3-phospho-L-serine, DOPS; 1-palmitoyl-2-oleoyl-*sn*-glycero-3-phospho-(1'-*rac*-glycerol), POPG; Small Unilamellar Vesicle, SUV; Large Unilamellar Vesicle, LUV; Multilamellar Vesicle, MLV; Size-Exclusion Chromatography, SEC; Circular Dichroism, CD; Nuclear Magnetic Resonance, NMR; Heteronuclear Single Quantum Coherence, HSQC; Dynamic Light Scattering, DLS; Isothermal Titration Calorimetry, ITC; Transmission Electron Microscopy, TEM; Matrix-Assisted Laser Desorption Ionization-Time Of Flight, MALDI-TOF; Fast Fourier Transform, FFT; ANalysis Of VAriance, ANOVA.

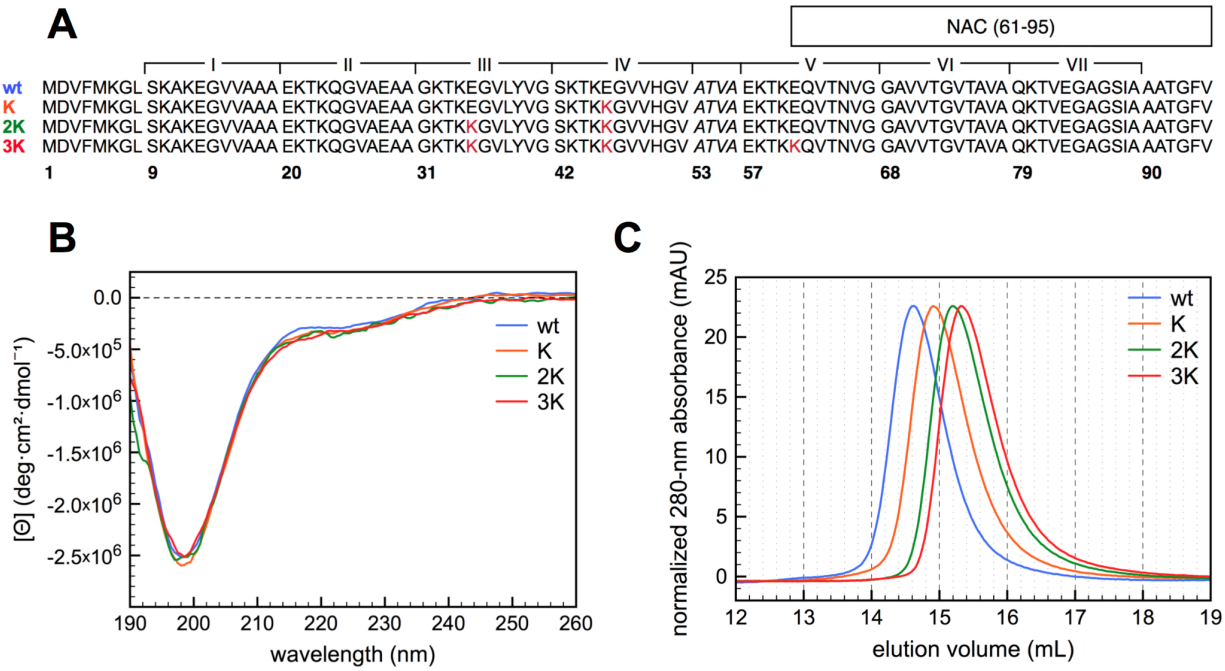

FIGURE 1. **Structural features of the E46K-like αSyn mutants in the lipid-unbound state.** *A*, Primary sequence of the N-terminal region (1-95) of wt, E46K ('K'), E35,46K ('2K'), and E35,46,61K ('3K') αSyn. E-to-K mutation sites are shown in red. The Non-Amyloid-β Component (NAC) domain (61-95) and the seven 11-mer repeats XKTKEGVXXXX are annotated on the sequence. *B*, Far-UV CD spectra of 10 μM wt, K, 2K and 3K αSyn in 10 mM NH_4Ac, pH 7.40, measured at 25ºC. The single minimum around 200 nm is characteristic of a predominantly unfolded ("random coil") secondary structure. *C*, Size-exclusion chromatography (Superdex 200 10/300 GL) of the E46K-like αSyn mutants, monitored by 280-nm absorbance (the absorbance signal shown in the chromatogram was normalized to equalize the peak heights). As a reference, an ovalbumin standard (44 kDa) elutes, on the same column, at 15.375 mL.

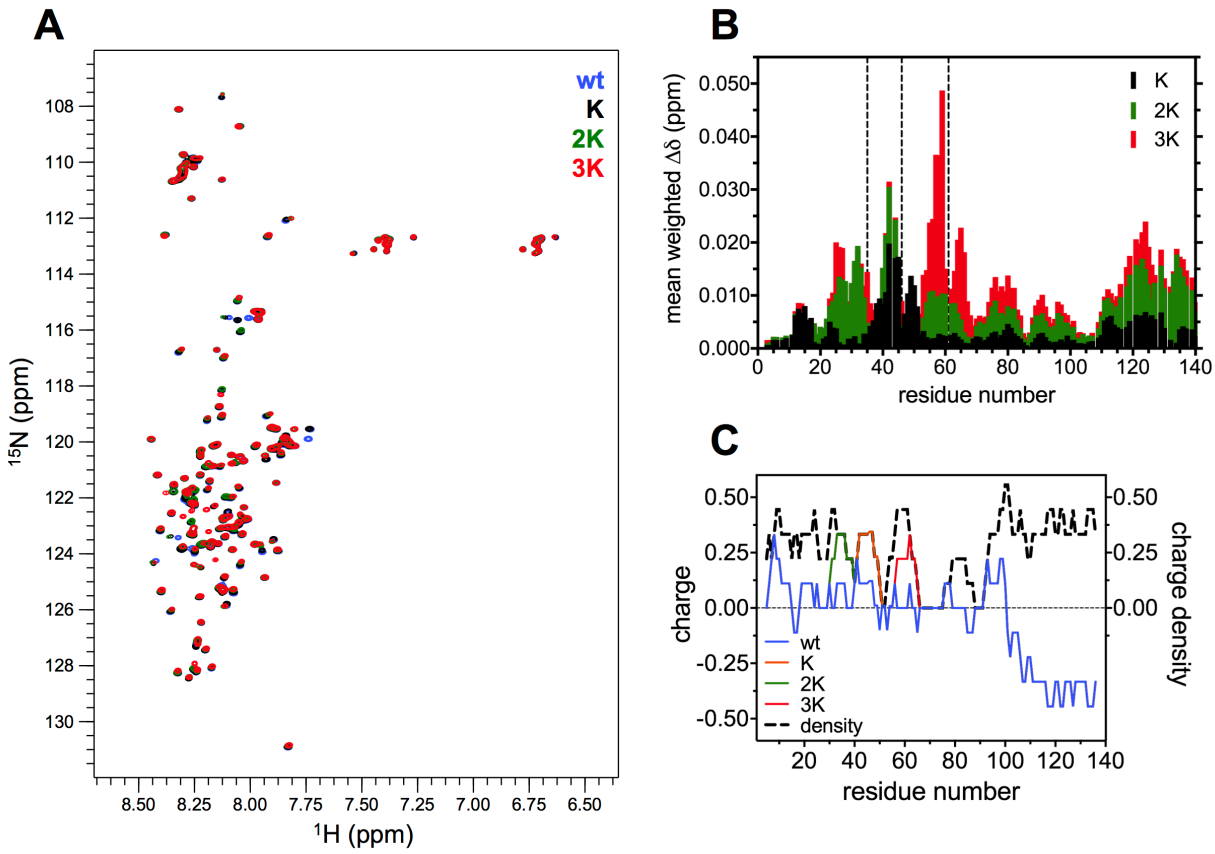

FIGURE 2. **NMR spectroscopy of the E46K-like αSyn mutants in the lipid-unbound state.** *A*, Overlaid ^{1}H-^{15}N HSQC spectra of 120 µM wt, K, 2K and 3K αSyn in 50 mM phosphate buffer, 10% D_2O, pH 6.80, measured at 15ºC, realigned using A140. *B*, Histogram of the mean weighted chemical shift perturbations (calculated as $[(\Delta\delta^{1}H)^2+(0.15\cdot\Delta\delta^{15}N)^2]^{1/2}$) of each mutant vs. wt αSyn, plotted against the corresponding residue number. In addition to the N-terminal region, the C-terminus is also affected and shows a clear correlation between the entity of the perturbations and the number of E-to-K mutations. *C*, Charge (and charge density, i.e. absolute charge value) distribution of wt αSyn and its mutants, averaged over a window of 9 amino acids. The transition from the N-terminal amphipathic region to the negatively charged C-terminus can be observed around residue 100. E-to-K mutations, while not changing the charge density distribution, increase the charge polarization, making electrostatic N-to-C interactions more favorable.

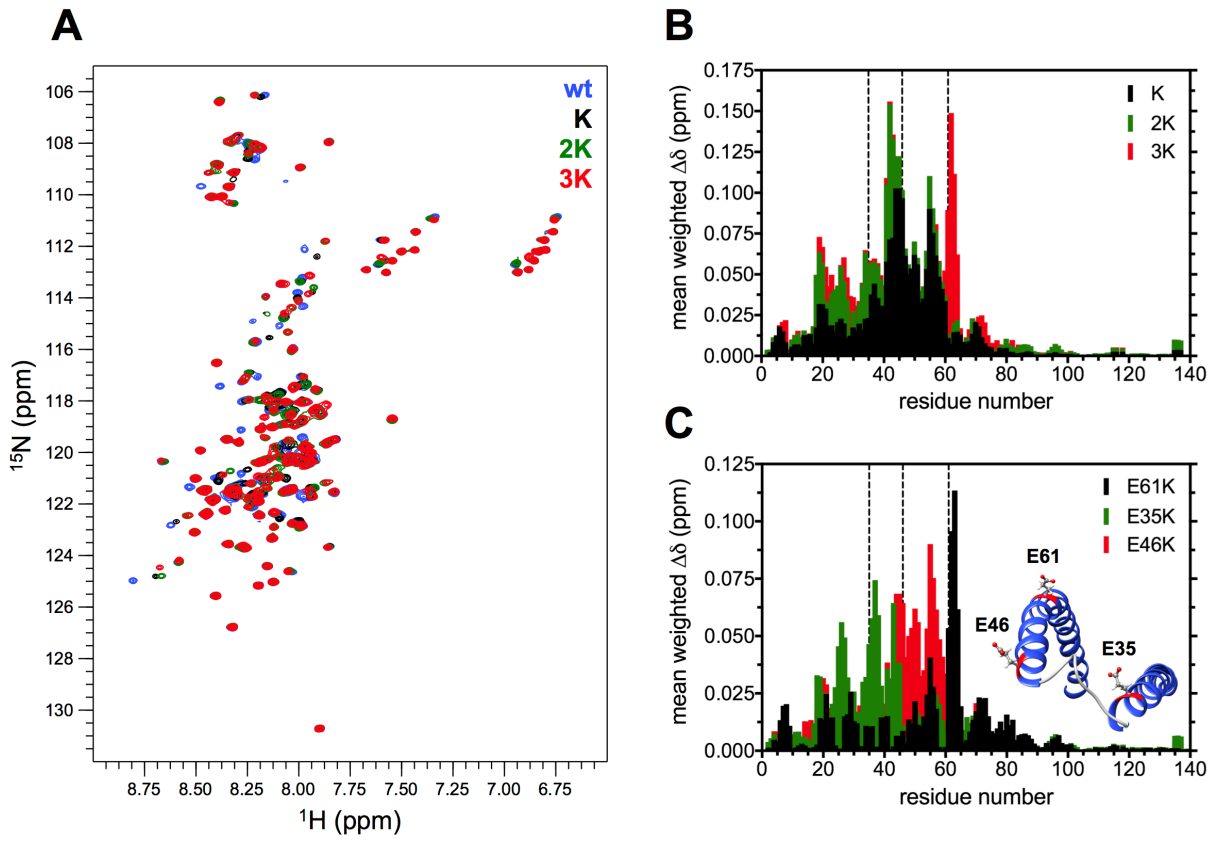

FIGURE 3. **NMR spectroscopy of the E46K-like αSyn mutants in the SDS-bound state.** *A*, Overlaid ^{1}H-^{15}N HSQC spectra of 120 μM wt, K, 2K and 3K αSyn in 15 mM SDS, 50 mM phosphate buffer, 10% D_2O, pH 6.80, measured at 37ºC, realigned using A140. *B*, Histogram of the mean weighted chemical shift perturbations (calculated as $[(\Delta\delta^{1}H)^2+(0.15\cdot\Delta\delta^{15}N)^2]^{1/2}$) of each mutant vs. wt αSyn, plotted against the corresponding residue number. *C*, Histogram of the mean weighted chemical shift perturbations of E46K vs. wt ('E46K'), 2K vs. E46K ('E35K'), 3K vs. 2K ('E61K'), plotted against the corresponding residue number. While the E35K and E46K mutations cause wide-ranging perturbations in the N-terminal region of SDS-bound αSyn, the effects of E61K are mostly clustered around the site of the mutation. This is easily understood upon examination of the deposited structure of SDS-bound αSyn (*inset* PDB: 1XQ8, showing the position and orientation of the glutamates in the sites of E-to-K mutation).

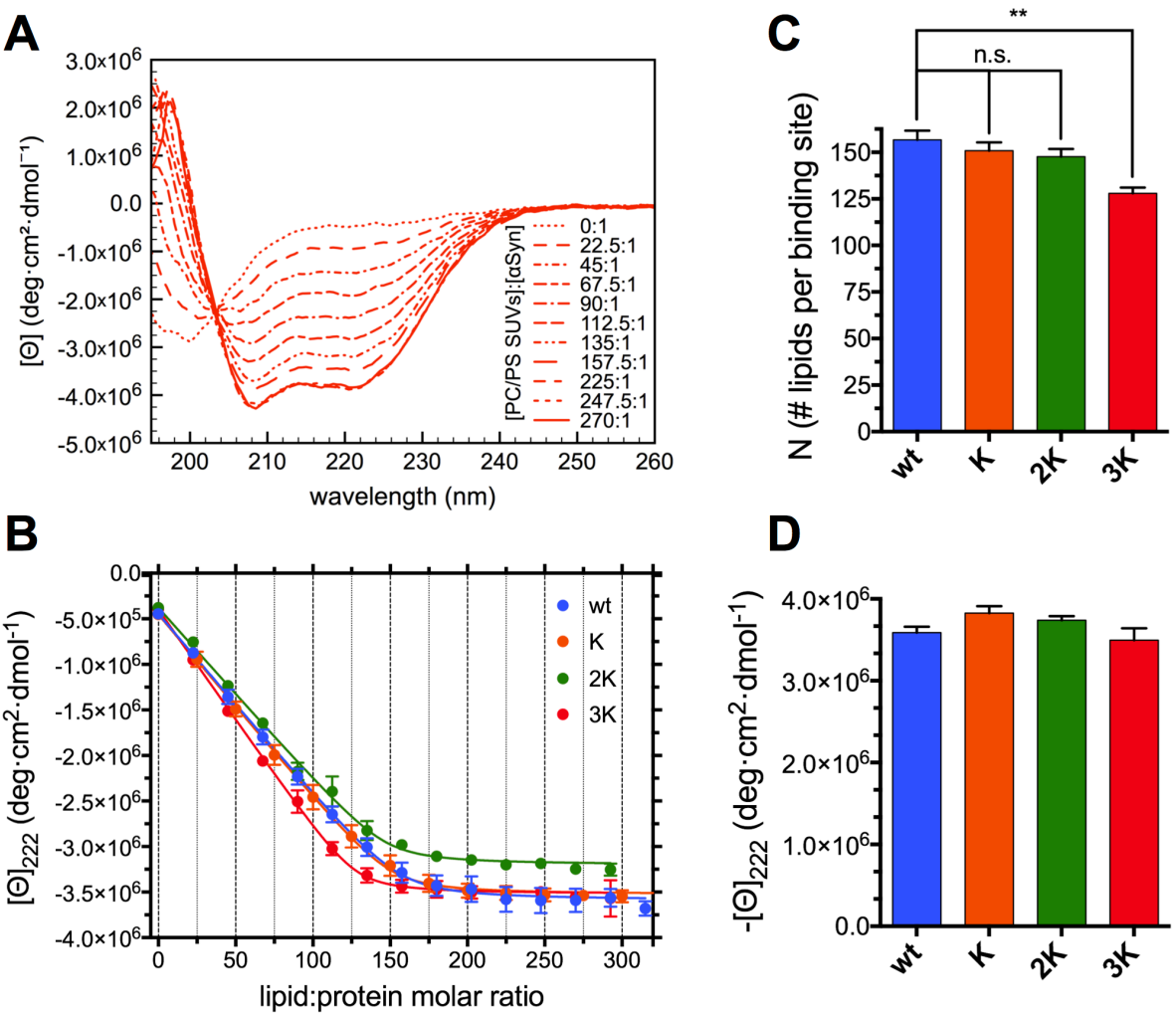

FIGURE 4. **E-to-K mutations result in mildly increased αSyn binding to curved charged membranes.** *A*, Representative far-UV CD spectra from a titration of 10 μM wt αSyn (in 10 mM NH_4Ac, pH 7.40) with 6 mM 70:30 POPC:DOPS SUVs, measured at 25ºC. There is a clear transition from the (almost completely) unstructured lipid-unbound protein to the robustly helical endpoints of the titration (e.g. lipid:protein molar ratio 270:1), reflecting the binding and folding of αSyn. *B*, Titration curves obtained from raw CD data after extracting the molar ellipticity at 222 nm and graphing it against the lipid:protein molar ratio at each point of the titration. Datapoints are shown along with their SEM (from *n*=3 independent titrations) and their best fit with an *N* independent binding sites model (*see* Experimental Procedures). *C*, Histogram of the *N* values (along with their SEM, *n*=3) obtained from the best fit of the titration curves with an *N* independent binding sites model. Decreasing *N*s indicate increased binding (or "avidity", *see* Results). *D*, Histogram of the 222-nm plateau molar ellipticity values (along with their SEM, *n*=3) obtained from the endpoint CD spectra of each mutant after renormalization using the wt αSyn isodichroic point.

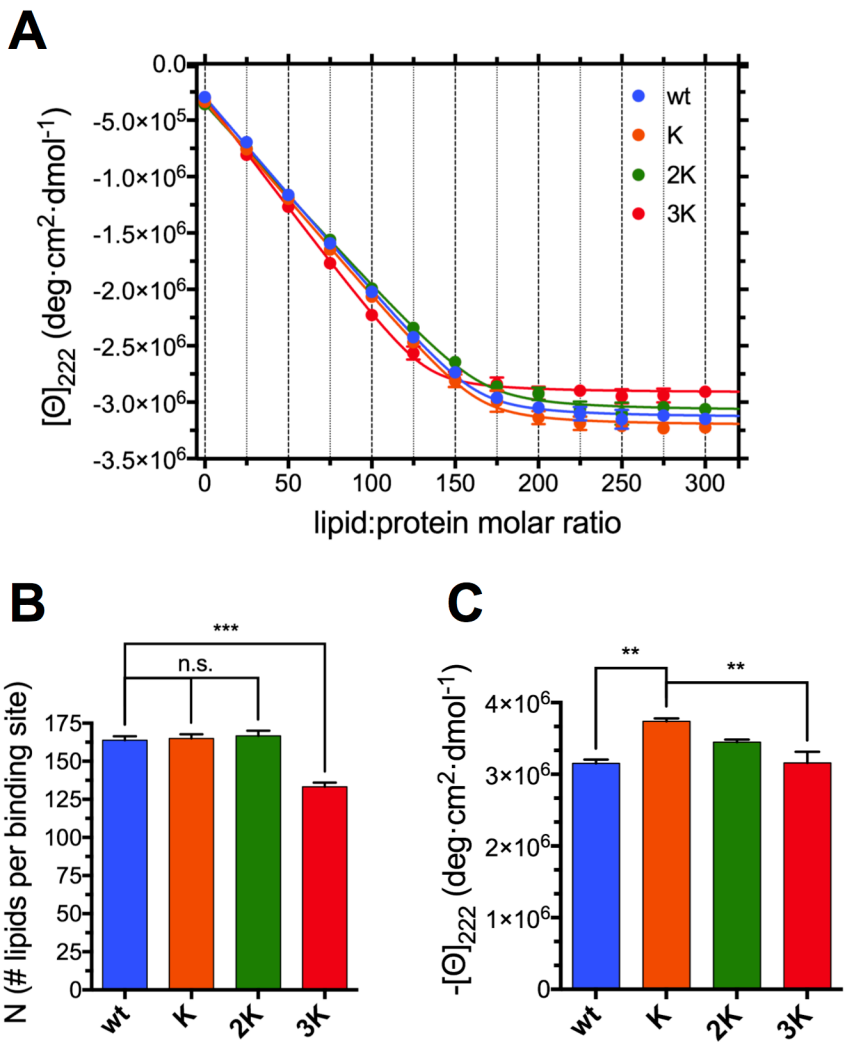

FIGURE 5. **E61K alone induces mildly increased binding to curved cholesterol-rich membranes.** *A*, Titration curves of 10 μM wt, K, 2K, and 3K αSyn (in 10 mM NH_4Ac, pH 7.40) with 6 mM 52.5:17.5:30 POPC:DOPS:cholesterol SUVs (measured at 25ºC). Plots were obtained from raw CD data after extracting the molar ellipticity at 222 nm and graphing it against the lipid:protein molar ratio at each point of the titration. Datapoints are shown along with their SEM (from n=3 independent titrations) and their best fit with an N independent binding sites model (*see* Experimental Procedures). *B*, Histogram of the N values (along with their SEM, n=3) obtained from the best fit of the titration curves with an N independent binding sites model. Decreasing Ns indicate increased binding (or "avidity", *see* Results). *C*, Histogram of the 222-nm plateau molar ellipticity values (along with their SEM, n=3) obtained from the endpoint CD spectra of each mutant after renormalization using the wt αSyn isodichroic point.

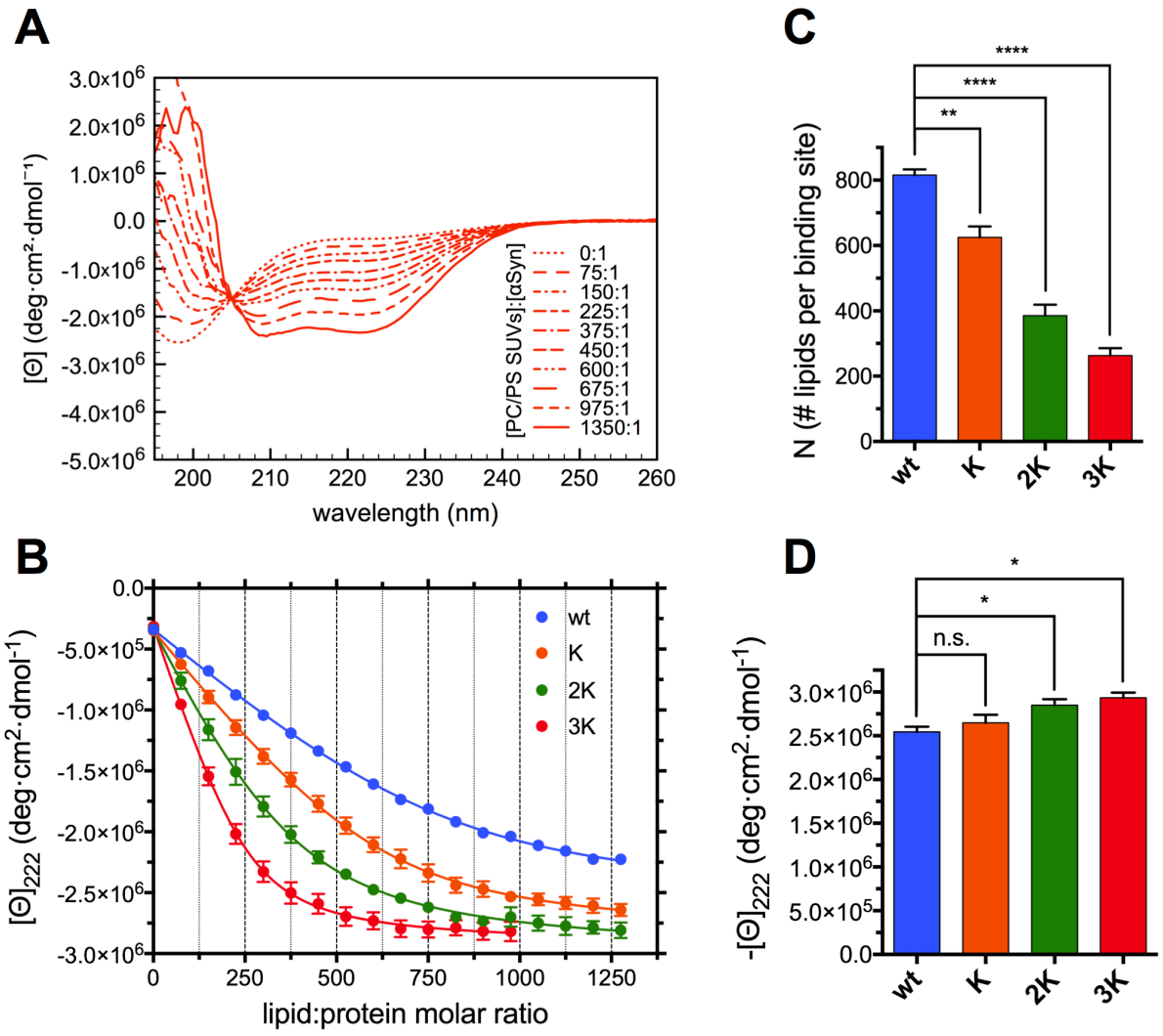

FIGURE 6. **αSyn's E-to-K mutations cause a progressive loss of curvature selectivity.** *A*, Representative far-UV CD spectra from a titration of 10 μM wt αSyn (in 10 mM NH_4Ac, pH 7.40) with 10 mM 70:30 POPC:DOPS LUVs, measured at 25ºC. While a coil-to-helix transition is also observed in the presence of LUVs, both its sharpness and the entity of the conformational rearrangement are much less than those observed with SUVs (*see* Fig. 4). *B*, Titration curves obtained from raw CD data after extracting the molar ellipticity at 222 nm and graphing it against the lipid:protein molar ratio at each point of the titration. Datapoints are shown along with their SEM (from *n*=3 independent titrations) and their best fit with an *N* independent binding sites model (*see* Experimental Procedures). *C*, Histogram of the *N* values (along with their SEM, *n*=3) obtained from the best fit of the titration curves with an *N* independent binding sites model. Decreasing *N*s indicate increased binding (or "avidity", *see* Results). *D*, Histogram of the 222-nm plateau molar ellipticity values (along with their SEM, *n*=3) obtained from the best fit of the titration curves after renormalization using the wt αSyn isodichroic point.

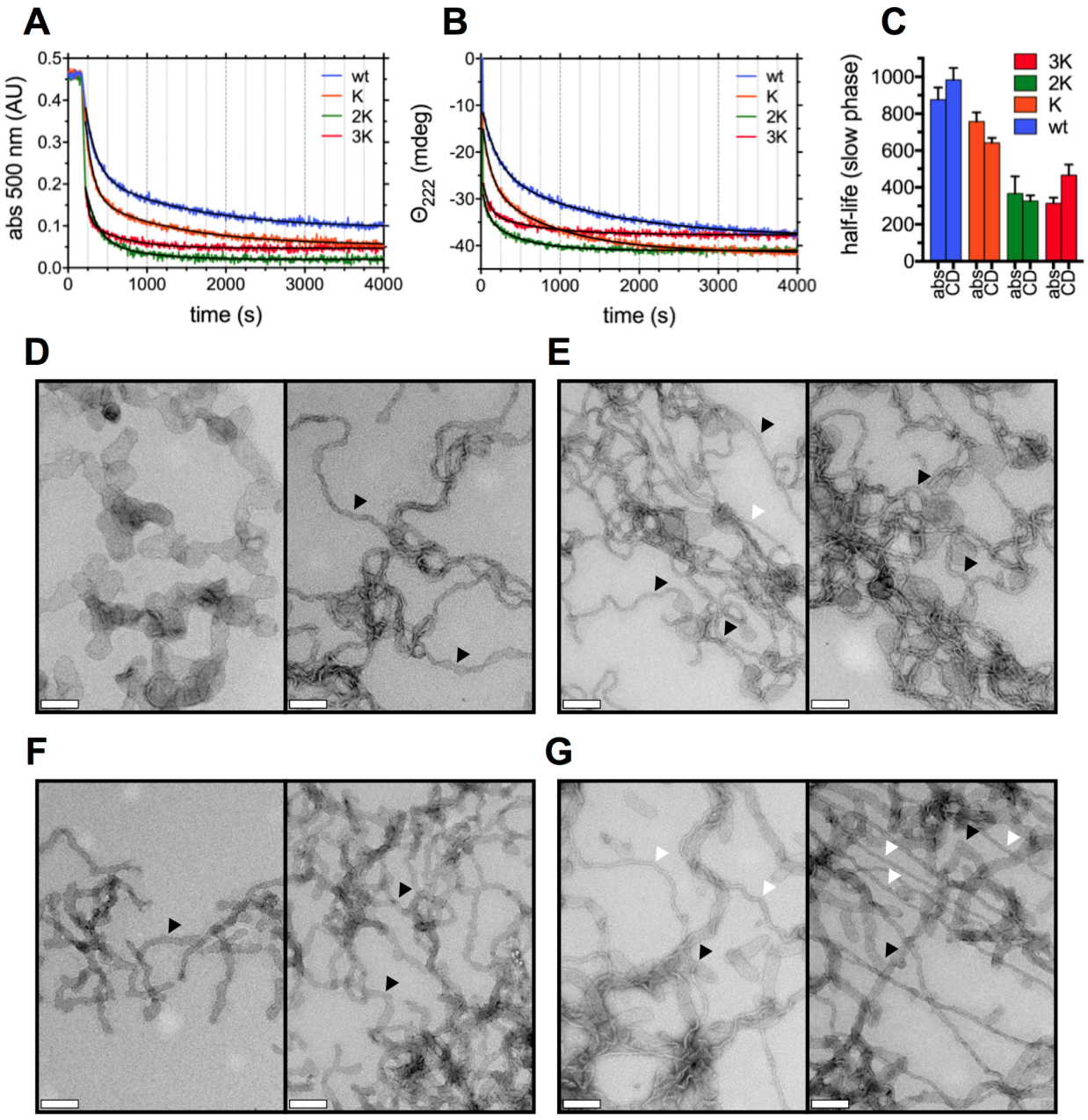

FIGURE 7. **αSyn's E-to-K mutations result in increased membrane remodeling.** *A*, Vesicle clearance experiments, monitored by absorbance at 500 nm, of 400 mM 90:10 POPG:POPC MLV dispersions by 40 μM wt αSyn and its E46K-like mutants (lipid:protein molar ratio 10:1). Best fits were obtained using a two-phase exponential decay model (*see* Table S3) and are shown in black. *B*, Vesicle clearance experiments, monitored by CD (222-nm ellipticity), of 400 mM 90:10 POPG:POPC MLV dispersions by 40 μM wt αSyn and its E46K-like mutants (lipid:protein molar ratio 10:1). Best fits were obtained as in (A) and are shown in black (*see* Table S3). *C*, Histogram of the (slow phase) half-life values (along with their 95% CI) obtained from the best fit of the clearance kinetics in (A) and (B) with a two-phase exponential decay model. As more E-to-K mutations are introduced, the clearance rate increases (and thus half-lives decrease), but the trend plateaus at 3K αSyn. *D-G*, Electron micrographs, negatively stained, of lipid tubule dispersions generated by mixing (D) wt, (E) E46K, (F) 2K, and (G) 3K αSyn to 90:10 POPG:POPC MLV preparations. Scale bar is 200 nm. While all mutants present the ability to robustly

tubulate membranes, with progressive E-to-K mutations the number of large, vesicular-like ‘cisternae’ (e.g D, left) and bilayer tubes (►) formed upon incubation with αSyn decreases and thinner, micellar (e.g. G, right) tubes are observed (▷).

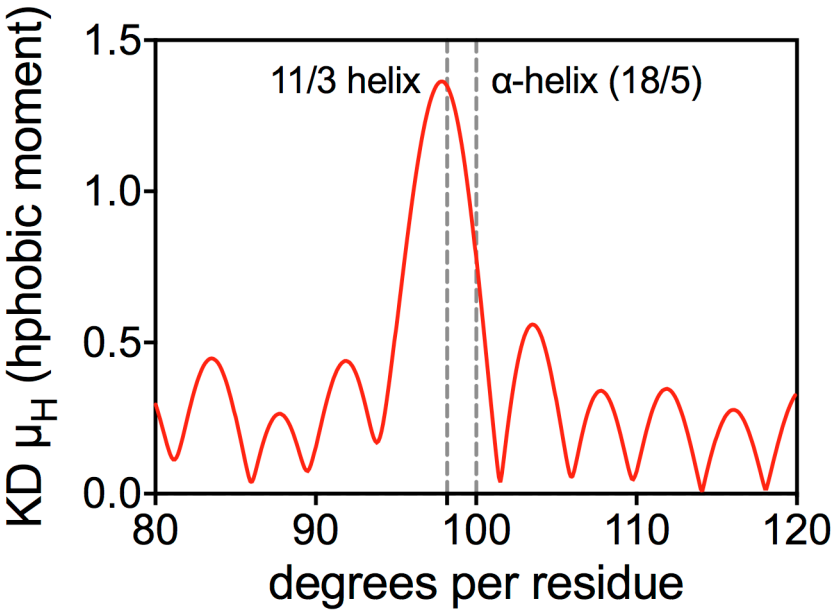

FIGURE 8. **αSyn's N-terminal region has an intrinsic propensity towards an 11/3 helix.** Hydrophobic moment, according to Eisenberg's definition (52), of the N-terminal segment of αSyn (1-95), calculated for different helix periodicities (using the hydropathy index values of Kyte and Doolittle (64)) and graphed against the angle between consecutive amino acids. The angles corresponding to an ideal α-helix (100º) and an ideal 11/3 helix (98.18º) are marked and labeled, showing how the amino acid arrangement in the N-terminus of αSyn leans towards an 11/3 arrangement if amphiphilicity (i.e. segregation of polar and apolar residues) is to be maximized.

E46K-like α-synuclein mutants increase lipid interactions and disrupt membrane selectivity

Matteo Rovere, Alex E. Powers, Haiyang Jiang, Julia C. Pitino, Luis Fonseca-Ornelas, Dushyant S. Patel, Alessandro Achille, Ralf Langen, Jobin Varkey and Tim Bartels

J. Biol. Chem. published online May 2, 2019
